Open access • Journal Article • DOI:10.1021/ACS.CHEMMATER.8B04278

Phenyl- and Pyrazolyl-Functionalized Pyrimidine: Versatile Chromophore of Bis-Tridentate Ir(III) Phosphors for Organic Light-Emitting Diodes — Source link

Yi-Kuang Chen, Hsin-Hung Kuo, Dian Luo, Yi-Ning Lai ...+7 more authors

Institutions: National Tsing Hua University, Yuan Ze University, Katholieke Universiteit Leuven, City University of Hong Kong

Published on: 10 Sep 2019 - Chemistry of Materials (American Chemical Society)

CHEMISTRY OF MATERIALS

Article

pubs.acs.org/cm

Phenyl- and Pyrazolyl-Functionalized Pyrimidine: Versatile Chromophore of Bis-Tridentate Ir(III) Phosphors for Organic Light-Emitting Diodes

Yi-Kuang Chen,[†] Hsin-Hung Kuo,[†] Dian Luo,[‡] Yi-Ning Lai,[‡] Wei-Cheng Li,[‡] Chih-Hao Chang,[‡] Daniel Escudero,[§] Alex K.-Y. Jen,[∥] Ling-Yang Hsu,[†] and Yun Chi*[,†,∥]

[†]Department of Chemistry and Frontier Research Center on Fundamental and Applied Sciences of Matters, National Tsing Hua University, Hsinchu 30013, Taiwan

[‡]Department of Photonics Engineering, Yuan Ze University, Chung-Li 32003, Taiwan

[§]Department of Chemistry, KU Leuven, Celestijnenlaan 200F, B-3001 Leuven, Belgium

[∥]Department of Materials Science and Engineering and Department of Chemistry, City University of Hong Kong, Hong Kong SAR

Supporting Information

ABSTRACT: There is growing interest in the bis-tridentate Ir(III) emitters as they are expected to display both improved emission efficiency and improved photostability. Herein, we turned to the new emitters **m2h-1**−**3** and **m6h-1**−**3**, bearing a pincer carbene ancillary and a chromophoric chelate derived from judiciously selected phenyl-pyrimidine-pyrazole entities $(pzm2h^F)H_2$ and $(pzm6h^F)H_2$, which differ in terms of the location of phenyl and pyrazole substituents on the central pyrimidine. Density functional theory calculations revealed a notable change in the spin density distribution from the pyrimidine-pyrazolate entity in **m2h** to the pyrimidine-phenyl fragment in **m6h**. As a consequence, the **m6h** emitters exhibited both shortened emission lifetimes and improved stabilities during extensive photolysis in solution, while corresponding organic light-emitting diodes (OLEDs) doped with green-emitting **m6h-1** and sky-blue-emitting **m6h-2** and **m6h-3** exhibited external quantum efficiencies of 17.6, 15.9, and 17.6%, respectively, superior to those of all of their **m2h** counterparts at a practical luminance of 10^3 cd/m^2. This finding suggests a new methodology for fine-tuning the electronic transition that is important to high-performance and durable phosphorescent OLEDs.

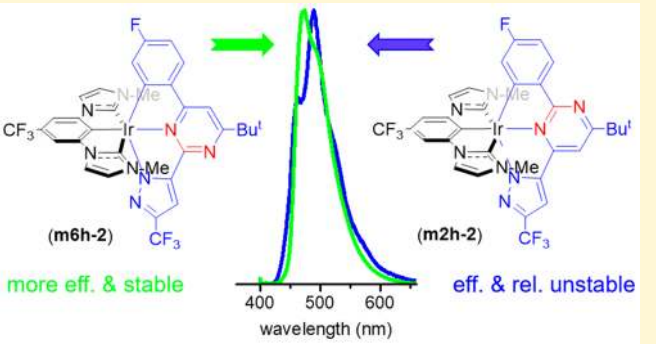

INTRODUCTION

Transition metal complexes have been widely studied in the context of efficient phosphors for organic light-emitting diodes (OLEDs),[1−8] which have already earned a pivotal position for both flat panel display and lighting applications. To further upgrade these next-generation technologies, it is essential to acquire durable and efficient materials (either transition metal-based phosphors or pure organic materials showing thermally activated delay fluorescence) that are capable of exhibiting efficient luminescence across the whole visible spectra, particularly in the blue region.[9−14] Among them, both green- and red-emitting phosphors have already passed stringent industrial assessments, because of their relatively decreased emission energies, and widely utilized for commercial applications. In sharp contrast, the development of blue-emitting phosphors lags behind because the greater emission energy for blue-emitting phosphors, along with their long triplet excited state lifetime, would induce notable sample decomposition during prolonged operation.[15−18] Moreover, an increase of the emitting excited state energy, which is needed to achieve blue emission, also reduces the energy separation between this emitting excited state and the upper-lying metal-centered (MC) dd states. These quenching states are capable of fostering a fast nonradiative decay, giving an unsatisfactory efficiency.[19−21] Notably, one method for blocking this nonradiative process is to employ metal phosphors with a bis-tridentate architecture,[22−24] for which the imposed higher rigidity and multiple metal−chelate coordination bonding are expected to offer higher ligand-field strength and, hence, a much destabilized MC dd excited state and more efficient blue emission.

Scheme 1 depicts the structural drawings of three typical sky-blue- and/or blue-emitting bis-tridentate Ir(III) phos-

Special Issue: Jean-Luc Bredas Festschrift

Received: October 9, 2018
Revised: November 23, 2018
Published: November 26, 2018

DOI: 10.1021/acs.chemmater.8b04278
Chem. Mater. XXXX, XXX, XXX−XXX

Scheme 1. Sky-Blue- and Blue-Emitting Bis-Tridentate Ir(III) Phosphors SB-tB, Px-5, and Cz-2

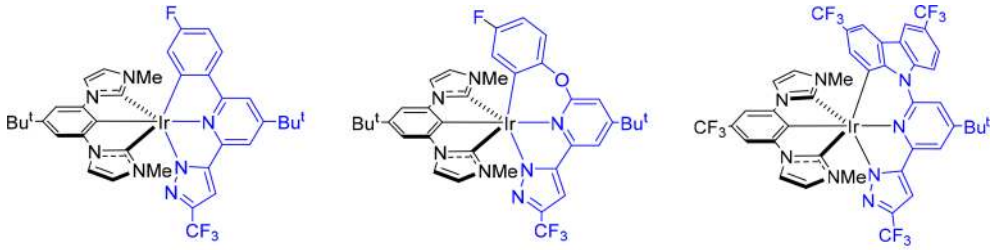

phors.[25,26] On one hand, all molecules share a common NHC carbene pincer chelate, which provides the strengthened ligand field for destabilizing the MC dd excited state needed for a higher emission efficiency. On the other hand, they exhibit a variety of chromophoric chelates bearing a central pyridyl unit that dominates the LUMOs of metal complexes. Therefore, replacement of this pyridyl entity with other heteroarene units, such as pyrimidine, is expected to bring forth a remarkable change in both chemical and photophysical properties.

In sharp contrast to N-heterocycles such as pyridine, pyrimidines are known for their strong electron accepting ability,[27] and hence, they are widely used as electron acceptors to construct thermally activated delayed fluorescence (TADF) emitters, with emission ranging from blue to green, a very high external quantum efficiency (EQE), and a slower efficiency roll-off at a high luminance.[28−34] Moreover, pyrimidine-containing organic materials have also been employed as components for electron transport material (ETM) to minimize driving voltages by increasing electron mobility and electron injection between the electron-transporting layer (ETL) and the emission layer (EML) of OLED devices.[35−38]

Pyrimidine has also been employed in the construction of transition metal-based phosphors. In a detailed study, Jiang, Liao, and co-workers designed and examined orange-emitting Ir(III) complexes with pyrimidine cyclometalates and obtained a maximum EQE of 28.2% for their emission efficiencies and horizontal transition dipole moments.[39] In developing better blue emitters, Shama et al. disclosed an anomalous phosphorescent OLED with a long operation lifetime, also featuring phenyl pyrimidinato cyclometalate Ir(III) complexes as dopant emittera.[40] Additional red-shifting of emission was achieved by functionalization of the 2-arylpyrimidine cyclometalate with an electron deficient 5-fluoro-substituted pyrimidine[41,42] or with a fused thieno[2,3-*d*]pyrimidine.[43] Upon using these Ir(III) complexes as dopant emitters, all OLED devices maintain adequately high EQEs. Moreover, changing from a 2-phenylpyrimidine to a 4,6-diphenylpyrimidine cyclometalate allows the fabrication of solution-processed OLEDs with high brightness, increased stability, and good efficiency.[44−46] All of these results suggest a key step forward in OLED performance through the introduction of pyrimidine in molecular design.

Encouraged by these findings, we were prompted to investigate the structure−property relationships of bis-tridentate Ir(III) complexes having pyrimidine functionality at the dianionic chromophoric chelate (cf. Scheme 2). Again, the higher electronegativity as well as the coordination orientation of N atoms on pyrimidine within these Ir(III) emitters is expected to impose a large difference on their inherent photophysical properties, such as emission color, efficiency, radiative lifetime, and stability upon excitation. These factors are of particular interest to the future design of durable and highly efficient phosphors for commercial OLED applications.

Scheme 2. Structural Drawings of Bis-Tridentate Ir(III) Metal Complexes m2h-1−3 and m6h-1−3 Bearing a Pyrimidinyl Functionality

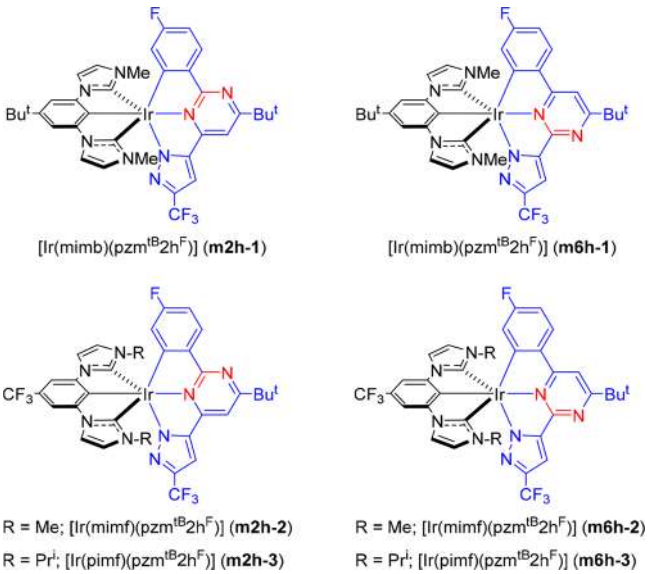

RESULTS AND DISCUSSION

Design and Syntheses. Preparation of the bis-tridentate Ir(III) requires two distinctive chelates, i.e., both monoanionic di-imidazolylidene pincer and dianionic chromophoric chelates. First, the dihexafluorophosphate salts of 1,3-bis(3-methylimidazolium-1-yl)-5-*tert*-butylbenzene $[(mimb)H_3\cdot(PF_6)_2]$, 1,3-bis(3-methylimidazolium-1-yl)-5-(trifluoromethyl)benzene $[(mimf)H_3\cdot(PF_6)_2]$, and 1,3-bis(3-isopropylimidazolium-1-yl)-5-(trifluoromethyl)benzene $[(pimf)H_3\cdot(PF_6)_2]$ were synthesized from 1,3-dibromo-5-*tert*-butylbenzene [or 1,3-dibromo-5-(trifluoromethyl)benzene] by addition of imidazole, followed by alkylation with methyl iodide (or isopropyl iodide) and anion metathesis according to literature procedures.[47] Scheme 3 depicts the structural drawings of these pincer chelates.

On the other hand, procedures giving the dianionic chromophoric chelates, i.e., $(pzy^{tB}ph^F)H_2$, $(pzm2h^F)H_2$, and $(pzm6h^F)H_2$, are presented in Scheme 4, for which full experimental details are provided in the Supporting Information. Briefly, the parent 2-phenyl-6-pyrazolylpyridine chelate $(pzy^{tB}ph^F)H_2$ was prepared by coupling of 1-[4-(*tert*-butyl)-6-

DOI: 10.1021/acs.chemmater.8b04278
Chem. Mater. XXXX, XXX, XXX−XXX

Scheme 3. Structural Drawings of Dicarbene Chelates Employed in This Study

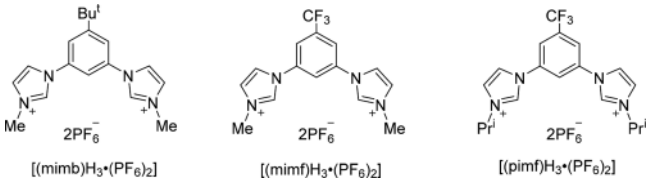

Scheme 4. Synthetic Routes to Chelates $(pzy^{tB}ph^{F})H_2$, $(pzm2h^{F})H_2$, and $(pzm6h^{F})H_2$[a]

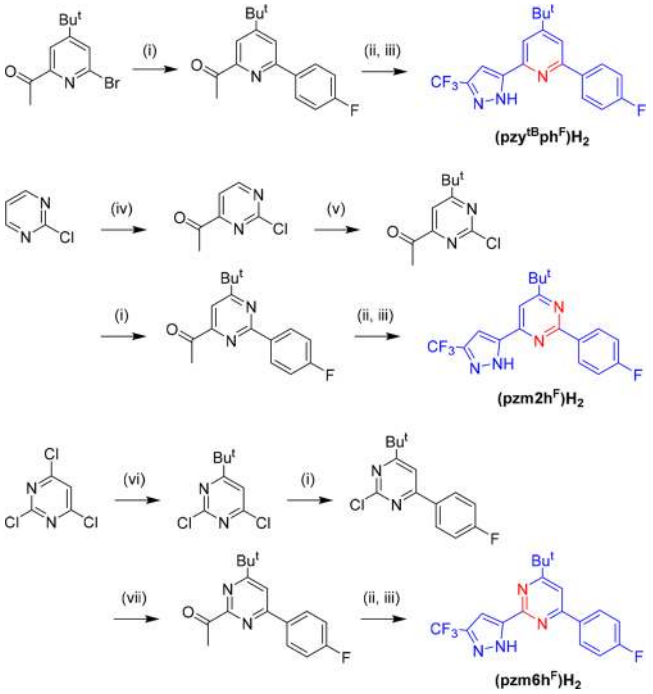

[a]Conditions: (i) 4-fluorophenylbronic acid, $Pd(PPh_3)_2Cl_2$, K_2CO_3, dioxane/H_2O, 90 °C; (ii) NaOEt, ethyl trifluoroacetate, THF, reflux; (iii) $N_2H_4{\cdot}H_2O$, *p*-TsOH, EtOH, reflux; (iv) pyruvic acid, $K_2S_2O_8$, $AgNO_3$, CH_2Cl_2/H_2O, reflux; (v) pivalic acid, $(NH_4)_2S_2O_8$, $AgNO_3$, H_2SO_4, H_2O, reflux; (vi) Bu^tMgBr, CuI, THF, room temperature; (vii) tributyl(1-ethoxyvinyl)tin, $Pd(PPh_3)_2Cl_2$, DMF, 90 °C.

chloropyridin-2-yl]ethan-1-one and 4-fluorophenylboronic acid to afford 1-[4-(*tert*-butyl)-6-(4-fluorophenyl)pyridin-2-yl]ethan-1-one. Then, Claisen condensation involving this intermediate and ethyl trifluoroacetate followed by hydrazine cyclization led to formation of $(pzy^{tB}ph^{F})H_2$ in high yield. For chelates with a pyrimidine skeletal framework, their key intermediates, namely, 1-[6-(*tert*-butyl)-2-(4-fluorophenyl)-pyrimidin-4-yl]ethan-1-one and 1-[4-(*tert*-butyl)-6-(4-fluorophenyl)pyrimidin-2-yl]ethan-1-one, were obtained from commercially available 2-chloropyrimidine and 2,4,6-trichloropyrimidine, respectively, via two distinctive multistep procedures. Next, they were treated with ethyl trifluoroacetate and with hydrazine using similar synthetic procedures to give two distinctive pyrimidine chelates, $(pzm2h^{F})H_2$ and $(pzm6h^{F})H_2$, respectively. Importantly, we have deliberately introduced a 4-substituted *tert*-butyl pyrimidinyl unit for all chelate designs. This modification is intended to control the regioselective coordination. Otherwise, the central pyrimidine fragment can use either N atom to initiate coordination, giving smaller synthetic yields or even dimetallic complexes with unexpected stoichiometries and photophysical properties.[48−51]

With these chelates in hand, all bis-tridentate Ir(III) complexes **SB-tB**, **m2h-1−3**, and **m6h-1−3** were synthesized using a one-pot synthetic approach, i.e., equal molar ratio of both chelates and $IrCl_3{\cdot}3H_2O$, together with excess K_2CO_3 in refluxing propionic acid; their structural drawings are depicted in Scheme 1. These Ir(III) complexes were purified using column chromatography, recrystallization, and sublimation. Mass spectrometry, elementary analyses, and both ^1H and ^{19}F nuclear magnetic resonance (NMR) analyses were conducted, for which the NMR assignments were determined by comparison with those of free chelates and previously reported Ir(III) metal complexes. Single-crystal X-ray analyses of Ir(III) complexes **m2h-1** and **m6h-1** were also examined. Their structural drawings are presented in Figures S1 and S2, exhibiting a slightly distorted pyrimidine fragment, and nearly planar architecture for both of the tridentate chelates expected for the bis-tridentate Ir(III) metal architecture.

Photophysical Data. Ultraviolet−visible (UV−vis) absorption spectra of all Ir(III) complexes **SB-tB**, **m2h-1−3**, and **m6h-1−3** were recorded in a CH_2Cl_2 solution at room temperature (RT), and their numerical data are summarized in Table 1. Figure 1 depicts the UV−vis absorption spectra of the first five Ir(III) complexes (**SB-tB**, **m2h-1**, **m2h-2**, **m6h-1**, and **m6h-2**), all with methyl-substituted imidazolylidene fragments. Ir(III) complexes **m2h-3** and **m6h-3** are isopropyl-substituted analogues of methyl complexes **m2h-2** and **m6h-2**, respectively, and hence, they are expected to exhibit similar spectral characters (cf. Figure S3) and are ignored for the sake of clarity. It is worth mentioning that all studied Ir(III) complexes show a similar absorption pattern in the <350 nm spectral region, which is attributed to the ligand-centered $\pi\pi^*$ excitations, among which the lowest-energy peak maximum

Table 1. Photophysical and Relevant Data of the Studied Ir(III) Metal Complexes

	absorbance λ_{max} (nm) ($\varepsilon \times 10^{-3}$)	emission λ_{max} (nm)[a]	Φ (%)[a]	τ_{obs} (μs)	Φ (%)[b]	τ_{obs} (μs)[b]	$E^{ox}_{1/2}$ (V)[c]	$E^{red}_{1/2}$ (V)	T_d (°C)[d]
SB-tB	279 (35), 329 (29), 382[4]	473, 504, 540(sh), 583(sh)	100	3.78	89	2.96	0.43 [0.08]	−2.71 [irr]	393.6
m2h-1	293 (29), 329 (20), 416 (2)	506	92	2.59	86	1.72	0.48 [0.06]	−2.74 [0.13]	397.2
m2h-2	291 (37), 326 (22), 394 (4)	462(sh), 489, 523(sh)	94	4.43	65	3.33	0.75 [0.08]	−2.71 [irr]	412.5
m2h-3	292 (38), 326 (22), 395 (4)	465(sh), 491	100	3.89	62	3.26	0.59 [0.09]	−2.66 [0.11]	379.2
m6h-1	290 (29), 329 (16), 391 (4)	515	96	0.93	100	1.08	0.37 [0.06]	−2.51 [0.11]	417.5
m6h-2	289 (25), 327 (13), 391 (3)	473, 498(sh)	97	1.52	76	1.28	0.67 [0.05]	−2.40 [0.11]	412.5
m6h-3	290 (31), 325 (15), 389 (3)	477, 498(sh)	100	1.53	81	1.33	0.62 [0.09]	−2.22 [0.12]	373.7

[a]Photophysical data were recorded in CH_2Cl_2 at a concentration of 10^{-5} M at RT. [b]Recorded at 8 wt % doped in a DEPEO thin film. [c]$E_{1/2}$ refers to $(E_{pa} + E_{pc})/2$, where E_{pa} and E_{pc} are the anodic and cathodic potentials, respectively, referenced to the redox couple (Fc/Fc$^+$ = −4.8 eV), while the corresponding values of $\Delta E_p = E_{pa} - E_{pc}$ are given in square brackets. [d]With a 5% weight loss.

DOI: 10.1021/acs.chemmater.8b04278
Chem. Mater. XXXX, XXX, XXX−XXX

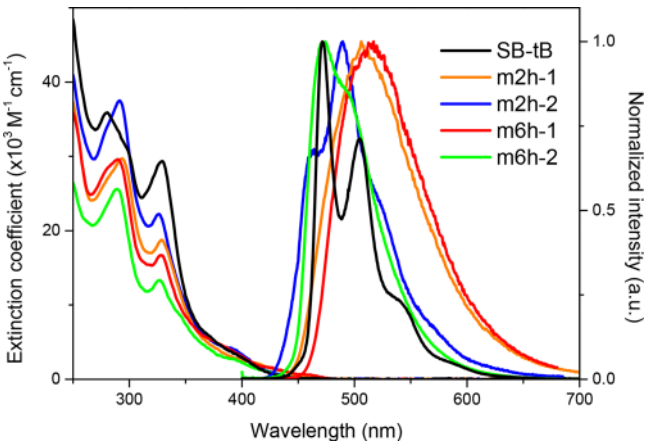

Figure 1. UV−vis absorption and normalized emission spectra of Ir(III) metal complexes recorded in a CH_2Cl_2 solution at RT.

appeared at ∼327 nm. Hence, changing the central pyridinyl unit to an isomeric pyrimidine has imposed indistinguishable variation on absorption bands. On the other hand, the less intense absorption beyond 425 nm is assigned to a mixed transition that contains both triplet ligand-centered $\pi\pi^*$ and metal-to-ligand charge transfer (MLCT) transitions. As depicted in Figure S4, Ir(III) complexes **m2h-1** and **m6h-1** display an intense red-shifted absorption band in this region, in comparison to that of **m2h-2** and **m6h-2**. These are clearly attributed to the electron-donating effect of the 4-*tert*-butylphenyl group on the mimb chelate, which lowers their MLCT transition energy via an increase in electron density at the central Ir(III) metal atom.

On the contrary, Ir(III) complexes **SB-tB**, **m2h-1**, **m2h-2**, **m6h-1**, and **m6h-2** exhibit very distinctive emission profiles. First, the parent complex **SB-tB** exhibits a structured emission with three peak maxima located at 473, 504, and 540 nm. Its unitary emission efficiency (Φ = 100%) and short lifetime (τ_{obs} = 3.78 μs) are consistent with phosphorescence enhanced by the rigidified bis-tridentate architecture. Upon replacement of the pyridinyl unit of **SB-tB** with both isomeric pyrimidinyl units in **m2h-1** and **m6h-1**, the emission band underwent a notable red-shift, together with a change in the emission profile to structureless and a decrease in the observed emission lifetime from 3.78 μs to 2.59 μs and 0.93 μs, respectively. This observation confirms the dominating MLCT character and, more importantly, a further decrease in the MLCT onset energy for **m6h-1** with the pzm6h^F chelate in reference to **m2h-1** bearing the pzm2h^F chelate.

Furthermore, substituting the electron-withdrawing CF_3 group at the pincer chelate causes a blue-shift and changes the emission profile back to structured, as observed for both **m2h-2** and **m6h-2** with Φ values of 94 and 97% and τ_{obs} values of 4.43 and 1.52 μs, respectively. Notably, a small red-shift in the emission onset energy exists for **m6h-2** compared to **m2h-2**. This trend was also found between **m6h-1** and **m2h-1**, implying a generalized decrease in emission energy for the pzm6h^F versus pzm2h^F chelates. Finally, complex **m6h-2** with a lowered emission onset exhibits a more dominate 0−0 transition band, while its counterpart **m2h-2** with a higher onset energy showed a reduced 0−0 transition intensity in comparison to the 0−1 transition intensity. This observation highlights a distinctive excited state character between these isomeric pyrimidinyl complexes and will be investigated in subsequent theoretical investigations.

Electrochemistry. Electrochemical data are measured using cyclic voltammetry, for which all data are presented in Table 1 and Figure S5. In general, all Ir(III) complexes showed reversible oxidation potentials, which are primarily associated with a central Ir(III) metal atom, among which **SB-tB**, **m2h-1**, and **m6h-1** bearing the pzy^{tB}ph^F, pzm2h^F, and pzm6h^F chromophoric chelated and identical mimb ancillary showed oxidation potentials of 0.43, 0.48, and 0.37 V, respectively. This trend implicates their general trend of electron donating character, i.e., pzm6h^F > pzy^{tB}ph^F > pzm2h^F, which seems to be independent to the number of N atoms involved in these chelates. Furthermore, similar variation of oxidation potentials is confirmed between Ir(III) complexes **m2h-2** and **m6h-2**, for which **m6h-2** with the pzm6h^F chelate also showed an oxidation potential at 0.67 V less positive than that of **m2h-2** (0.75 V) bearing the pzm2h^F chelate and an identical mimf ancillary, but the trend turns less obvious between **m2h-3** and **m6h-3** bearing the pimf ancillary, which may be attributed to the stronger electron donating effect of the isopropyl group to the central Ir(III) cation while it bears the pzm2h^F chelate. Overall, this means that the electron density at the Ir(III) metal atom increases in the following order: **m2h-1** < **SB-tB** < **m6h-1** and **m2h-2** < **m6h-2**; i.e., pzm2h^F and pzm6h^F chelates induce the lowest and greatest electron density at the Ir(III) metal center. Moreover, those with an identical pzm2h^F or pzm6h^F chromophoric chelate showed systematic increases in their oxidation potentials, i.e., 0.48 V (**m2h-1**) < 0.59 V (**m2h-3**) < 0.75 V (**m2h-2**), and 0.37 V (**m6h-1**) < 0.62 V (**m6h-3**) < 0.67 V (**m6h-2**), which are in accord with the relative electron donor character of pincer ancillaries, e.g., mimb > pimf > mimf, toward the Ir(III) metal center.

On the contrary, those with the pzm6h^F chelate consistently showed reduction potentials that were lower than the potentials of those bearing the pzm2h^F chelate and an identical pincer ancillary (e.g., −2.74 and −2.53 V for **m2h-1** and **m6h-1**, −2.71 and −2.40 V for **m2h-2** and **m6h-2**, and −2.66 and −2.22 V for **m2h-3** and **m6h-3**, respectively) as well as reduction in the electrochemical gap, i.e., the difference between their redox potentials, confirming the detected red-shifting in emission for Ir(III) complexes **m6h-1**, **m6h-2**, and **m6h-3** in comparison to that of their isomeric counterparts **m2h-1**, **m2h-2**, and **m2h-3**, respectively.

Photostability. All these pyrimidine-based Ir(III) complexes display high T_d values obtained from thermogravimetric analysis (TGA) (cf. Table 1 and Figure S6). In an attempt to test their stability under more stringent conditions, we perform the photodegradation study under irradiation with a xenon discharging lamp at 620 W/m^2 and at a constant temperature of 35 °C. Figure 2 presents the plots of emission intensity of the studied Ir(III) complexes in degassed toluene versus irradiation time. It is believed that the recorded emission intensity should be proportional to the remaining concentration of the analyte after photolysis. Hence, the rate constants (k) for the photoinduced decomposition reaction can be obtained using the integrated first-order rate law:

$$\ln\left[\frac{A_t}{A_0}\right] = -kt$$

The corresponding rate constants were next estimated to be 2.6 × 10^{-3} h^{-1} for [Ir(ppy)$_3$], 3.7 × 10^{-3} h^{-1} for **SB-tB**, and

DOI: 10.1021/acs.chemmater.8b04278
Chem. Mater. XXXX, XXX, XXX−XXX

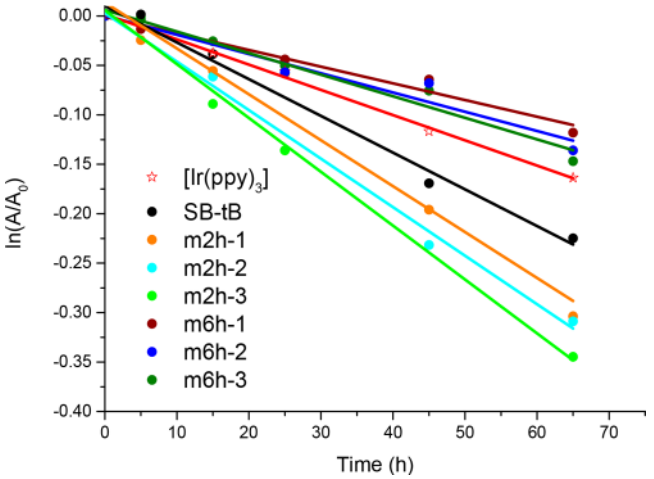

Figure 2. Photodegradation responses of Ir(III) emitters and reference *fac*-[Ir(ppy)$_3$], for which all samples were dissolved in deaerated toluene (concentration of 5×10^{-5} M), placed in an argon-filled PL cuvette, and subjected to simulated solar irradiation at 620 W/m^2 at a constant temperature of 35 °C.

4.6, 4.9, and 5.5×10^{-3} h^{-1} for **m2h-1**, **m2h-2**, and **m2h-3**, respectively, as well as 1.7, 2.0, and 2.2×10^{-3} h^{-1} for **m6h-1**, **m6h-2**, and **m6h-3**, respectively. From these data, we conclude that the members of the **m6h** series are slightly more photostable than the reference [Ir(ppy)$_3$] and **SB-tB** complexes. Unfortunately, the **m2h** series of emitters showed faster decomposition rate constants, which are approximately 2 times faster than that of their **m6h** counterparts. Because all studied pyrimidine-based emitters possess nearly identical emission quantum yields, the faster decomposition observed for **m2h** emitters should be attributed to the longer emission lifetime observed (2.59−4.43 μs) versus those of the **m6h** series of emitters (0.93−1.52 μs). This observation is also in good agreement with a recent report that the shortened exciton lifetime in the S$_1$ state is a key factor for realization of efficient blue-emitting TADF OLEDs.[52]

Theoretical Investigation. We performed density functional theory (DFT) calculations on selected bis-tridentate phosphors to gain further insights into their emissive properties. First, we aimed to disentangle the different emissive characteristics between the **m2h** and **m6h** series. Thus, complexes of the **m2h** series (**1** and **2**) and of the **m6h** series (**1** and **2**) were selected for the theoretical study. The geometries of the lowest triplet excited states, i.e., T$_1$, were optimized with UB3LYP, and the phosphorescence emission maxima were simulated on the basis of ΔSCF-B3LYP calculations at the T$_1$ minima (see the computational details in the Experimental Section). The computed emission maxima are 522, 473, 495, and 490 nm for **m2h-1**, **m2h-2**, **m6h-1**, and **m6h-2**, respectively, which correlate fairly well with the experimental evidence. The spin density (SD) distributions at the T$_1$ minima along with the SD at the Ir(III) atom are shown in Figure 3. Notably, the spin density plots evidence the greater participation of the pyrimidine-pyrazolate unit for **m2h-1** and **m2h-2** and the pyrimidine-phenyl unit for **m6h-1** and **m6h-2**, which provide hints about the notable difference in both the emission lifetime and photostability observed earlier. The altered photophysical data of the **m6h** series in comparison to those of the **m2h** series are reminiscent of the higher emission quantum yields observed in the facially coordinated Ir(III) metal complexes versus those of their meridional counterparts.[53−56]

Moreover, according to the SD at the Ir(III) metal atom, the MLCT character of T$_1$ increases in the following order: **m2h-2** (0.21) < **m6h-2** (0.23) < **m6h-1** (0.27) < **m2h-1** (0.42). The values in parentheses stand for the SD at the Ir(III) atoms. The SD plots at T$_1$ also evidence strong mixing between MLCT and ligand-based [i.e., ligand-centered (LC) and/or ligand-to-ligand charge transfer (LLCT)] excited states. For **m2h-2** (and **m6h-2**), the T$_1$ state is of mixed ^{3}MLCT/^{3}LC(pzm2(6)h^F) character. Conversely, in the case of **m2h-1** and **m6h-1**, their

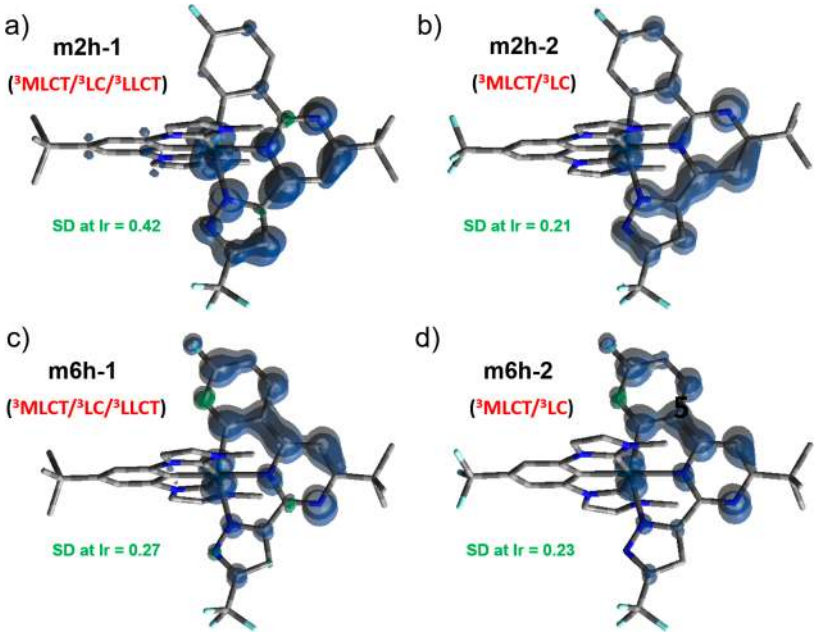

Figure 3. Spin density (SD) distributions at the T$_1$ minima of (a) **m2h-1**, (b) **m2h-2**, (c) **m6h-1**, and (d) **m6h-2**. The SD at the Ir atom is also highlighted.

DOI: 10.1021/acs.chemmater.8b04278
Chem. Mater. XXXX, XXX, XXX−XXX

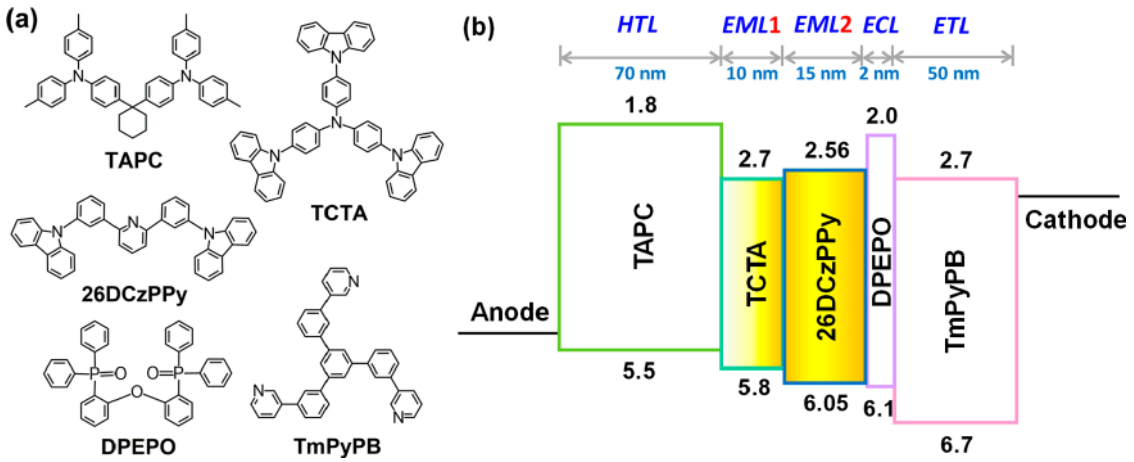

Figure 4. (a) Structural drawings of the OLED materials employed in this study. (b) Energy level diagram of the OLED devices.

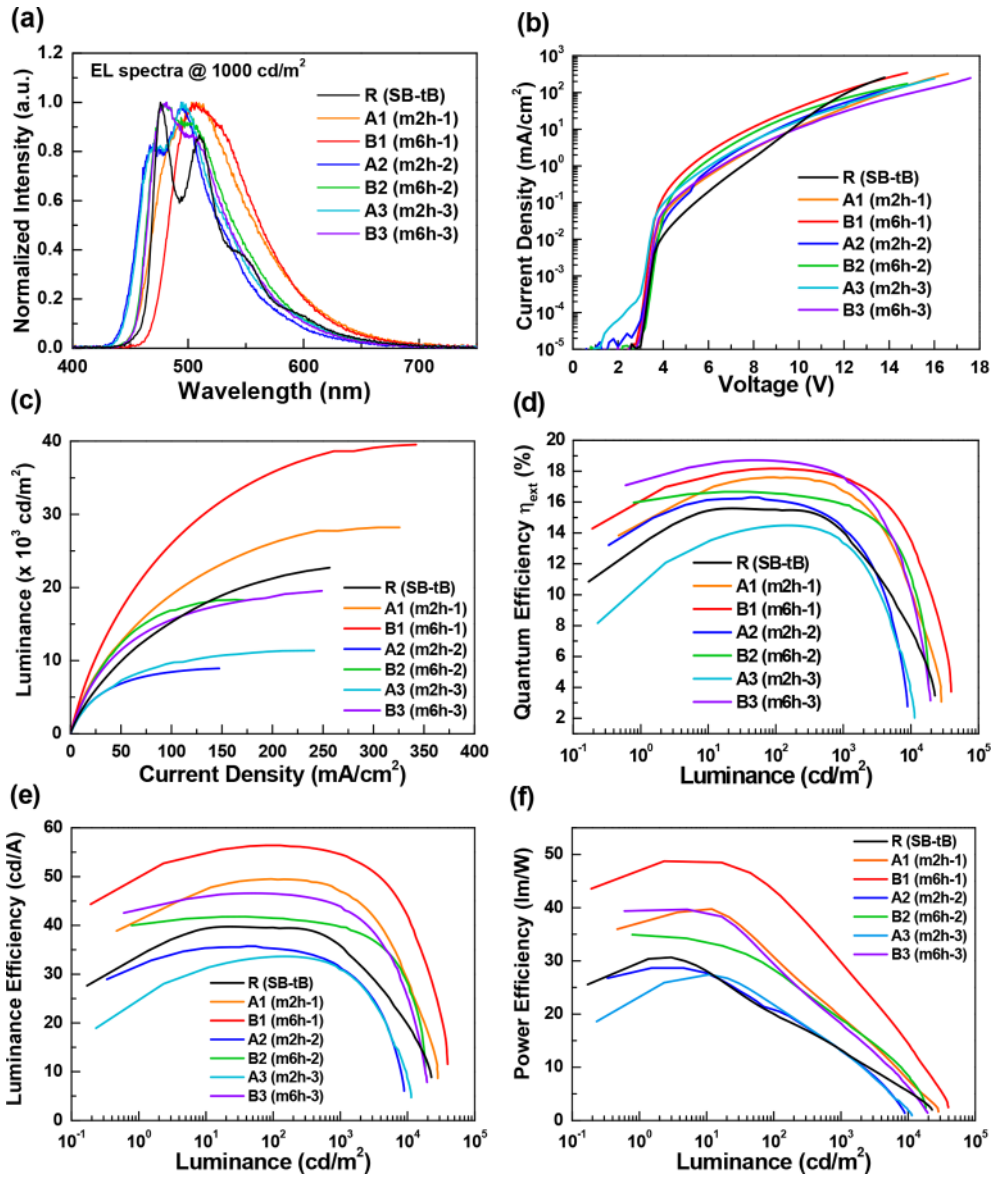

Figure 5. EL characteristics of OLEDs with fabricated emitters: (a) normalized EL spectra, (b) current density−voltage (J−V) characteristics, (c) current density−luminance (J−L) characteristics, (d) external quantum efficiency vs luminance, (e) luminance efficiency vs luminance, and (f) power efficiency vs luminance for devices A1, B1, A2, B2, A3, and B3.

DOI: 10.1021/acs.chemmater.8b04278
Chem. Mater. XXXX, XXX, XXX−XXX

Table 2. EL Characteristics of Studied OLEDs with the Ir(III) Emitter at a Concentration of 8 wt %

	R, **SB-tB**	A1, **m2h-1**	A2, **m2h-2**	A3, **m2h-3**	B1, **m6h-1**	B2, **m6h-2**	B3, **m6h-3**
EQE (%)							
maximum efficiency	15.6	17.6	16.2	14.5	18.2	16.7	18.7
recorded at 10^2 cd/m^2	15.5	17.6	16.1	14.5	18.2	16.6	18.7
measured at 10^3 cd/m^2	14.1	16.7	14.3	13.3	17.6	15.9	17.6
LE (cd/A)							
maximum efficiency	39.8	49.5	35.7	33.6	56.4	41.8	46.6
recorded at 10^2 cd/m^2	39.5	49.5	35.3	33.6	56.4	41.5	46.5
measured at 10^3 cd/m^2	35.8	47.0	31.4	30.9	54.6	39.7	43.9
PE (lm/W)							
maximum efficiency	30.6	39.8	28.7	27.4	48.7	34.9	39.7
recorded at 10^2 cd/m^2	20.0	30.8	20.9	21.8	43.4	28.3	29.5
measured at 10^3 cd/m^2	13.3	19.5	13.1	13.1	29.8	19.0	18.2
V_{on}[a] (V)	3.5	3.4	3.5	3.3	3.3	3.6	3.4
maximum luminance (cd/m^2) [V]	22705 [13.8]	28219 [16.6]	8924 [14.2]	11378 [16.0]	39528 [14.8]	18224 [14.8]	19531 [17.6]
λ_{max}[b] (nm)	476	503	494	496	507	481	481
CIE 1931 coordinates							
recorded at 10^2 cd/m^2	(0.23, 0.46)	(0.26, 0.50)	(0.18, 0.36)	(0.21, 0.39)	(0.28, 0.58)	(0.21, 0.45)	(0.21, 0.44)
measured at 10^3 cd/m^2	(0.22, 0.46)	(0.25, 0.50)	(0.18, 0.36)	(0.20, 0.38)	(0.27, 0.58)	(0.21, 0.44)	(0.20, 0.43)

[a]Turn-on voltage measured at 1 cd/m^2. [b]Measured at 10^3 cd/m^2.

T_1 states also exhibit certain LLCT character, which is more pronounced in the case of **m2h-1** (see the residual SD in their mimb-based chelates in panels a and b of Figure 3). Certainly, the substitution with an electron-donating *tert*-butyl group at the mimb-based chelate in **m2h-1** and **m6h-1** leads to (i) the co-participation of this ligand in the emission and (ii) an increase in the MLCT character of their T_1 states. These are the ultimate reasons that lead to red-shifted structureless emissions for **m2h-1** and **m6h-1**. Conversely, for **m2h-2** and **m6h-2** and because of their increased ^{3}LC, their emission bands are more structured. Comparison of the **m6h** and **m2h** series with the previously reported **SB-tB** complex (see its computed SD distribution in Figure S7) reveals, first, the reduced MLCT character of its T_1 state [because the SD at the Ir(III) amounts to only 0.10] and, second, a larger involvement of the pyrimidine-pyrazolate unit in the emission process. The lower MLCT character of the T_1 state of **SB-tB** leads to longer excited state lifetimes as compared to those obtained for the **m6h** and **m2h** series. Because of their reduced lifetimes, the use of the latter complexes might be beneficial for diminishing efficiency roll-off effects and/or degradation processes.

Electroluminescence. The electroluminescence (EL) devices were investigated by doping the studied Ir(III) emitters into several selected host materials. In addition, the device with **SB-tB** was also prepared for comparison. Considering their emission colors ranging from sky-blue to green, the host materials with a triplet energy bandgap higher than 2.8 eV should be suitable for offering effective exothermic host−guest energy transfer. Furthermore, double emitting layers (DEMLs) were employed to control the exciton formation zone, offering adequate carrier recombination as well as convenient adjustment of carrier balance.[57,58] In general, the DEMLs are constructed using two hosts with opposite carrier transport capabilities (i.e., electron and hole), aiming to provide better carrier balance and to improve carrier recombination.[57,58] However, most carriers would recombine at the corresponding EML interface and increase the exciton concentration in a narrow space, giving an increased level of triplet−triplet annihilation (TTA).[59,60] Therefore, we employed a pair of host materials with good hole transport ability and bipolar property, aiming to mitigate the TTA phenomenon.[61,62] Herein, 4,4′,4″-tris(carbazol-9-yl)triphenylamine (TCTA) was adopted as the first EML with good hole transport ability, while the bipolar 2,6-bis[3-(9*H*-carbazol-9-yl)phenyl]pyridine (26DCzPPy) was employed as the second EML.[63−66] The hole mobility of TCTA was estimated to be 10^{-4} cm^2 V^{-1} s^{-1}, whereas 26DCzPPy possesses similar hole and electron mobilities of 10^{-5} cm^2 V^{-1} s^{-1}.[63−66] In addition, a wide triplet-energy-bandgap material, bis[2-(diphenylphosphino)phenyl]ether oxide (DPEPO),[67,68] was chosen as a thin exciton-confining layer (ECL) located between the EML and electron transport layer (ETL), facilitating exciton confinement as well as carrier adjustment.[69,70] Because of the poor electron mobility of DPEPO, a thin layer of DPEPO (2 nm) was employed to alleviate its negative impact on electron transport. Moreover, 1,1-bis[(di-4-tolylamino)phenyl]cyclohexane (TAPC) and 1,3,5-tri[(3-pyridyl)phen-3-yl]benzene (TmPyPB) were adopted as the hole transport layer (HTL) and the ETL, because of their high transport capabilities of 1×10^{-2} and 1×10^{-3} cm^2 V^{-1} s^{-1} and high triplet gaps (E_T) of 2.87 and 2.78 eV, respectively.[71−74] Their layer thicknesses and dopant concentrations were also carefully regulated to enhance carrier balance and radiation output. As a result, the optimal performance was obtained with a doping concentration of 8 wt %. Consequently, the device architecture was finalized as ITO (120 nm)/TAPC (70 nm)/TCTA and 8 wt % emitters (10 nm)/26DCzPPy and 8 wt % emitters (15 nm)/DPEPO (2 nm)/TmPyPB (50 nm)/LiF (0.8 nm)/Al (150 nm), for which LiF and aluminum were used as the electron injection layer and reflective cathode, respectively. Panels a and b of Figure 4 show the chemical structure of the employed materials and energy level diagram, respectively.

The EL of the fabricated devices and the numerical data are summarized in Figure 5 and Table 2. It is notable that the first EML with a better hole-transporting TCTA host facilitated carrier recombination near the TCTA/26DCzPPy interface. In addition, the bipolar 26DCzPPy host would cause the exciton to be evenly distributed over the second EML, and the ECL with DPEPO with the higher triplet gap was needed to limit

DOI: 10.1021/acs.chemmater.8b04278
Chem. Mater. XXXX, XXX, XXX−XXX

exciton diffusion. Figure 5a depicts the normalized EL spectra of these devices measured at a luminance of 10^3 cd/m^2. As indicated, all EL spectra exhibited solely the emitters' emission, demonstrating adequate exciton confinement.[67,68] Furthermore, no host emission was observed in the EL spectra, indicating the effective host−guest energy transfer at the employed doping concentration.[75] As shown in Figure 5b, the current density−voltage (J−V) curves revealed that devices B1 and B2 with emitters **m6h-1** and **m6h-2** possessed current densities relatively higher than those of devices A1 and A2 with the **m2h-1** and **m2h-2** counterparts, but device B3 with **m6h-3** exhibited a current density slightly lower than that of device A2 with **m2h-3**. These outcomes illustrated the combined effect of both the pyrimidinyl unit and carbene pincer ancillary on carrier transport. Moreover, both series of devices A and B exhibited current density that was superior to that of device R with **SB-tB**, which may result from the higher electron mobility of the pyrimidine unit.

On the other hand, as shown in Figure 5c, the respective maximum luminances of devices B1−B3 were recorded as 39528, 18224, and 19531 cd/m^2, respectively, which were much higher than those of devices A1−A3, which had maximum luminances of 28219, 8924, and 11378 cd/m^2, respectively. This is because human eyes respond more strongly to the green emission, and hence, green-emitting devices A1 and B1 produced luminances much higher than those of the sky-blue- and blue-emitting devices.[76]

Panels d−f of Figure 5 show the EQE, luminance efficiency (LE), and power efficiency (PE) versus luminance, indicating higher efficiencies for the **m6h**-based devices in response to their **m2h** counterparts. The peak EQE, LE, and PE of green-emitting device A1 with **m2h-1** were recorded as 17.6% (49.5 cd/A and 39.8 lm/W), while device B1 with **m6h-1** exhibited higher peak efficiencies of 18.2% (56.4 cd/A and 48.7 lm/W). In addition, the peak efficiencies of devices A2, A3, B2, and B3 with blue emitters **m2h-2**, **m2h-3**, **m6h-2**, and **m6h-3** reached 16.2% (35.7 cd/A and 28.7 lm/W), 14.5% (33.6 cd/A and 27.4 lm/W), 16.7% (41.8 cd/A and 34.9 lm/W), and 18.7% (46.6 cd/A and 39.7 lm/W), respectively. These data were relatively better than those of device R (cf. maximum EQE, LE, and PE values of 15.6% (39.8 cd/A and 30.6 lm/W), indicating the practical advantage of these bis-tridentate molecules with pyrimidine units. Again, the higher PLQY of the **m6h**-based emitters and the better carrier balance achieved in all devices B have had a significant influence on the obtained EL efficiencies. Hence, green-emitting **m2h-1** and **m6h-1** maintained forward efficiencies of 17.6% (16.7%) and 18.2% (17.6%) at a practical brightness of 10^2 cd/m^2 (10^3 cd/m^2). Furthermore, slightly lowered peak (or maximum) EQEs of 15.5% (14.1%), 16.1% (14.3%), 16.6% (15.9%), 14.5% (13.3%), and 18.7% (17.6%) were obtained for the corresponding blue-emitting OLED devices R, A2, B2, A3, and B3, respectively, at a practical luminance of 10^2 cd/m^2 (10^3 cd/m^2). As a result, the efficiency decay at 10^3 cd/m^2 from their peak value was estimated to be 11, 5−12, and 3−6% for devices R, A1−A3, and B1−B3, respectively. In addition, the estimated declines in EQE by one-half were obtained at current densities ($J_{1/2}$) of 49.5, 52.3, 30.5, 34.9, 82.8, 71.1, and 47.9 mA/cm^2 for reference device R and tested devices A1−A3 and B1−B3, respectively.[77,78] Clearly, the efficiency roll-off observed in these devices was insignificant, confirming that the adopted double EMLs have effectively regulated the exciton distribution. Therefore, the enlarged exciton formation zone in the double EMLs has diluted the triplet exciton concentration in space and then mitigated both TTA and polaron quenching.[79,80] On closer inspection of these results, all devices B with **m6h**-based emitters exhibited less obvious efficiency roll-off compared to that of devices A with **m2h**-based emitters, due to the shorter emission lifetimes. Overall, the superior performance of devices B demonstrated the high potential of these **m6h**-based Ir(III) emitters in all potential OLED applications.

CONCLUSION

In summary, we synthesized two series of bis-tridentate Ir(III) emitters, **m2h-1−3** and **m6h-1−3**, bearing a pair of pincer carbene ancillary and two distinctive phenyl-pyrimidine-pyrazole chromophoric chelates, i.e., (pzm2h^F)H$_2$ and (pzm6h^F)H$_2$, in which their phenyl and pyrazole substituents are located at two opposite sides of the central pyrimidine fragment. First, pyrimidine was selected because of its enhanced electron accepting character in comparison to that of pyridine and its better capacitance in giving enhanced MLCT transition character at the excited states and improved efficiencies for the as-fabricated OLED devices. Second, there is a notable change in the spin density distribution from the pyrimidine-pyrazolate entity in **m2h** to the pyrimidine-phenyl fragment in **m6h**, as revealed by DFT calculations. These results are in good agreement with the observed photophysical data, in which all **m6h** emitters exhibited both shortened emission lifetimes in solution and as doped thin films, and with improved stability under extended UV−vis photolysis. The OLEDs doped with green-emitting **m6h-1** and sky-blue-emitting **m6h-2** and **m6h-3** exhibited maximum EQEs of 17.6, 15.9, and 17.6%, respectively, which are all superior to those of their **m2h** counterparts with maximum EQEs of 16.7, 14.3, and 13.3%, respectively, at a luminance of 10^3 cd/m^2. This finding suggests a new method for fine-tuning the electronic transition process that is critical for attaining highly efficient and durable phosphorescent OLEDs.

EXPERIMENTAL SECTION

General Information and Materials. All reactions were conducted under a N_2 atmosphere, and solvents were dried and distilled prior to use. Commercially available reagents were used without further purification. ^{1}H and ^{19}F NMR spectra were measured with Varian Mercury-400 and Varian Mercury-500 instruments. Elemental analysis was performed on a Heraeus CHN-O rapid elementary analyzer. Mass spectra were recorded on a JEOL model JMS-T200GC AccuTOF GCx instrument operating in electron impact (EI) or field desorption (FD) mode. Cyclic voltammetry was performed using a model CHI621A electrochemical analyzer. The potentials are measured with a Ag/Ag$^+$ reference electrode together with a Pt electrode with 0.1 M NBu_4PF_6 in CH_2Cl_2 or a gold working electrode with 0.1 M NBu_4PF_6 in THF. The reported data are referenced to the ferrocenium/ferrocene (Fc^+/Fc) couple.

Synthesis of pzm2ph^F and pzm6ph^F Chelates. Two related pyrimidine-based chelates, i.e., 4-(*tert*-butyl)-2-(4-fluorophenyl)-6-[3-(trifluoromethyl)-1*H*-pyrazol-5-yl]pyrimidine (pzm2h^{F}H$_2$) and 4-(*tert*-butyl)-6-(4-fluorophenyl)-2-[5-(trifluoromethyl)-1*H*-pyrazol-3-yl]pyrimidine (pzm6h^{F}H$_2$) substituted pyrimidine, are synthesized using synthetic procedures depicted in the Supporting Information.

General Procedure for the Bis-Tridentate Ir(III) Complexes. As a general procedure, a mixture of [(mimb)H$_3$·(PF$_6$)$_2$] (176 mg, 0.3 mmol), (pzm2h^F)H$_2$ (**L2**, 108 mg, 0.3 mmol), $IrCl_3·3H_2O$ (105 mg, 0.3 mmol), and K_2CO_3 (829 mg, 6.0 mmol) was dissolved in propionic acid (30 mL) and refluxed under nitrogen for 12 h. After the mixture had cooled to RT, the solvent was removed *in vacuo*. The residue was extracted into ethyl acetate (50 mL), washed with brine

DOI: 10.1021/acs.chemmater.8b04278
Chem. Mater. XXXX, XXX, XXX−XXX

(30 mL) three times, dried over anhydrous Na_2SO_4, and concentrated. The crude product was purified by column chromatography eluting with a mixture of ethyl acetate and hexane (1:3 to 1:1) to give a light-yellow solid of **m2h-1** (yield of 89 mg, 0.11 mmol, 35%). Ir(III) derivatives **m2h-2**, **m2h-3**, **m6h-1**, and **m6h-3** were obtained in 28−33% yields, while **SB-tB** was obtained from a mixture of $[(mimb)H_3{\cdot}(PF_6)_2]$, $(pzy^{tB}ph^{F})H_2$, and $IrCl_3{\cdot}3H_2O$ under similar conditions.

Selected Spectral Data of ***SB-tB***. ^{1}H NMR (400 MHz, DMSO-d_6, 25 °C): δ 8.13 (d, J = 1.6 Hz, 2H), 7.97 (s, 2H), 7.92 (dd, J = 8.4 Hz, J = 6.0 Hz, 1H), 7.59 (s, 2H), 7.22 (s, 1H), 6.99 (d, J = 1.6 Hz, 2H), 6.48 (td, J = 8.4 Hz, J = 2.4 Hz, 1H), 5.19 (dd, J = 9.6 Hz, J = 2.4 Hz, 1H), 2.66 (s, 6H), 1.49 (s, 9H), 1.47 (s, 9H). ^{19}F−{^{1}H} NMR (376 MHz, DMSO-d_6, 25 °C): δ −58.04 (s, 3F), −112.34 (s, 1F). MS (LRFD): $[M + H]^+$ 847.3. Anal. Calcd for $C_{37}H_{36}F_4IrN_7$: C, 52.47; H, 4.28; N, 11.58. Found: C, 52.23; H, 4.07; N, 11.44.

Selected Spectral Data of ***m2h-1***. ^{1}H NMR (500 MHz, DMSO-d_6, 80 °C): δ 8.06 (d, J = 2.0 Hz, 2H), 7.99−7.96 (m, 2H), 7.58 (s, 2H), 7.39 (s, 1H), 6.96 (d, J = 2.0 Hz, 2H), 6.56 (td, J = 8.8 Hz, J = 2.7 Hz, 1H), 5.31 (dd, J = 9.6 Hz, J = 2.7 Hz, 1H), 2.67 (s, 6H), 1.52 (s, 9H), 1.51 (s, 9H). ^{19}F−{^{1}H} NMR (470 MHz, DMSO-d_6, 80 °C): δ −58.38 (s, 3F), −109.72 (s, 1F). MS (LRFD): $[M + H]^+$ 848.2. Anal. Calcd for $C_{36}H_{35}F_7IrN_8$: C, 50.99; H, 4.16; N, 13.22. Found: C, 50.39; H, 4.50; N, 12.90.

Selected Crystal Data of ***m2h-1***. $C_{72}H_{72}F_8Ir_2N_{16}O$; M = 1713.85; monoclinic; space group $P2_1/c$; a = 12.9918(5) Å, b = 24.4505(9) Å, c = 22.1009(9) Å; β = 91.4855(11)°; V = 7018.1(5) Å^3; Z = 4; ρ_{Calcd} = 1.622 Mg m^{-3}; $F(000)$ = 3400; crystal size of 0.312 mm × 0.177 mm × 0.165 mm; λ(Mo Kα) = 0.71073 Å; T = 150(2) K; μ = 3.866 mm^{-1}; 45928 reflections collected, 16093 independent reflections (R_{int} = 0.0339), maximum and minimum transmission of 0.7456 and 0.6495, respectively; data/restraints/parameters = 16093/6/930; GOF = 1.049; final R_1 [$I > 2\sigma(I)$] = 0.0254 and wR_2 (all data) = 0.0552; CIF data deposited as CCDC entry 187240.

Selected Spectral Data of ***m2h-2***. ^{1}H NMR (500 MHz, DMSO-d_6, 80 °C): δ 8.22 (d, J = 2.1 Hz, 2H), 8.02−7.99 (m, 2H), 7.92 (s, 2H), 7.42 (s, 1H), 7.05 (d, J = 2.1 Hz, 2H), 6.60 (td, J = 8.9 Hz, J = 2.5 Hz, 1H), 5.23 (dd, J = 9.6 Hz, J = 2.5 Hz, 1H), 2.73 (s, 6H), 1.53 (s, 9H). ^{19}F−{^{1}H} NMR (470 MHz, DMSO-d_6, 80 °C): δ −58.24 (s, 3F), −58.52 (s, 3F), −109.31 (s, 1F). MS (LRFD): $[M + H]^+$ 860.3. Anal. Calcd for $C_{33}H_{26}F_7IrN_8$: C, 46.10; H, 3.05; N, 13.03. Found: C, 45.83; H, 3.45; N, 12.70.

Selected Spectral Data of ***m2h-3***. ^{1}H NMR (500 MHz, DMSO-d_6, 80 °C): δ 8.29 (d, J = 2.1 Hz, 2H), 8.02 (s, 1H), 7.99 (dd, J = 8.5 Hz, J = 6.5 Hz, 1H), 7.93 (s, 2H), 7.40 (s, 1H), 7.26 (d, J = 2.1 Hz, 2H), 6.58 (td, J = 8.5 Hz, J = 2.6 Hz, 1H), 5.24 (dd, J = 9.6 Hz, J = 2.6 Hz, 1H), 3.07 (sept, J = 6.8 Hz, 2H), 1.54 (s, 9H), 0.68 (d, J = 6.8 Hz, 6H), 0.65 (d, J = 6.8 Hz, 6H). ^{19}F−{^{1}H} NMR (470 MHz, DMSO-d_6, 80 °C): δ −58.25 (s, 3F), −58.66 (s, 3F), −109.22 (s, 1F). MS (LRFD): $[M + H]^+$ 916.1. Anal. Calcd for $C_{37}H_{34}F_7IrN_8$: C, 48.52; H, 3.74; N, 12.23. Found: C, 48.29; H, 4.07; N, 12.38.

Selected Spectral Data of ***m6h-1***. ^{1}H NMR (500 MHz, DMSO-d_6, 80 °C): δ 8.10−8.07 (m, 3H), 7.97 (s, 1H), 7.59 (s, 2H), 7.04 (s, 1H), 6.97 (d, J = 2.0 Hz, 2H), 6.63 (td, J = 8.8 Hz, J = 2.7 Hz, 1H), 5.33 (dd, J = 9.6 Hz, J = 2.7 Hz, 1H), 2.68 (s, 6H), 1.52 (s, 18H). ^{19}F−{^{1}H} NMR (470 MHz, DMSO-d_6, 80 °C): δ −58.32 (s, 3F), −109.10 (s, 1F). MS (LRFD): $[M + H]^+$ 848.1. Anal. Calcd for $C_{36}H_{35}F_7IrN_8$: C, 50.99; H, 4.16; N, 13.22. Found: C, 50.99; H, 4.00; N, 13.28.

Selected Crystal Data of ***m6h-1***. $C_{36}H_{35}F_4IrN_8$; M = 1183.95; monoclinic; space group $P2_1/n$; a = 12.3992(4) Å, b = 17.0920(5) Å, c = 17.1949(5) Å; β = 109.5160(8)°; V = 3434.71(18) Å^3; Z = 4; ρ_{Calcd} = 1.640 Mg m^{-3}; $F(000)$ = 1680; crystal size of 0.154 mm × 0.141 mm × 0.075 mm; λ(Mo Kα) = 0.71073 Å; T = 150(2) K; μ = 3.012 mm^{-1}; 27121 reflections collected, 7879 independent reflections (R_{int} = 0.0314), maximum and minimum transmission of 0.7456 and 0.6321, respectively; data/restraints/parameters = 7879/34/471; GOF = 1.082; final R_1 [$I > 2\sigma(I)$] = 0.0243 and wR_2 (all data) = 0.0542; CIF data deposited as CCDC entry 187239.

Selected Spectral Data of ***m6h-2***. ^{1}H NMR (500 MHz, DMSO-d_6, 80 °C): δ 8.23 (d, J = 2.0 Hz, 2H), 8.16 (dd, J = 8.7 Hz, J = 6.0 Hz, 1H), 8.01 (s, 1H), 7.93 (s, 2H), 7.05 (d, J = 2.0 Hz, 3H), 6.61 (td, J = 8.7 Hz, J = 2.6 Hz, 1H), 5.25 (dd, J = 9.6 Hz, J = 2.6 Hz, 1H), 2.74 (s, 6H), 1.52 (s, 9H). ^{19}F−{^{1}H} NMR (470 MHz, DMSO-d_6, 80 °C): δ −58.25 (s, 3F), −58.45 (s, 3F), −108.70 (s, 1F). MS (LRFD): $[M + H]^+$ 860.1. Anal. Calcd for $C_{33}H_{26}F_7IrN_8$: C, 46.10; H, 3.05; N, 13.03. Found: C, 46.35; H, 2.97; N, 13.18.

Selected Spectral Data of ***m6h-3***. ^{1}H NMR (500 MHz, DMSO-d_6, 80 °C): δ 8.30 (d, J = 2.1 Hz, 2H), 8.12 (dd, J = 9.0 Hz, J = 7.5 Hz, 1H), 8.01 (s, 1H), 7.93 (s, 2H), 7.26 (d, J = 2.1 Hz, 2H), 7.04 (s, 1H), 6.60 (td, J = 9.0 Hz, J = 3.0 Hz, 1H), 5.27 (dd, J = 10.0 Hz, J = 3.0 Hz, 1H), 3.07 (sept, J = 6.8 Hz, 2H), 1.54 (s, 9H), 0.69 (d, J = 6.8 Hz, 6H), 0.67 (d, J = 6.8 Hz, 6H). ^{19}F−{^{1}H} NMR (470 MHz, DMSO-d_6, 80 °C): δ −58.25 (s, 3F), −58.58 (s, 3F), −108.58 (s, 1F). MS (LRFD): $[M + H]^+$ 916.1. Anal. Calcd for $C_{37}H_{34}F_7IrN_8$: C, 48.52; H, 3.74; N, 12.23. Found: C, 48.86; H, 3.69; N, 12.28.

OLED Fabrication. Organic materials and the indium tin oxide (ITO)-coated glass were purchased from Lumtec and Shine Materials Technology. All organic materials were subjected to temperature gradient sublimation. The ITO substrate was washed with deionized water and acetone in sequence, followed by treatment with UV radiation and ozone for 5 min. The organic and metal layers were deposited onto the ITO-coated glass substrate by thermal evaporation, and device fabrication was completed in a single cycle without breaking the vacuum. A shadow mask was used to define the active area (2 mm × 2 mm) of the device. Current density−voltage−luminance characterization was performed using two Keithley 2401 current source-measure units equipped with a calibrated Si photodiode. The electroluminescence spectra were recorded using an Ocean Optics spectrometer.

Computational Details. All calculations were performed with DFT. The geometries of the singlet ground state and of the lowest triplet ES (T_1) were optimized using the B3LYP hybrid exchange-correlation functional[81,82] in combination with the 6-31G(d) atomic basis set for all atoms but the metal centers. Relativistic effects were included for Ir atoms by using the ecp-mwb-60 pseudopotentials.[83] The nature of the stationary points was confirmed by computing the Hessian at the same level of theory. The phosphorescence emission maxima were modeled on the basis of SCF-B3LYP calculations at the T_1 optimized geometries. The latter calculations were performed within the PCM framework (CH_2Cl_2 was used as a solvent).[84] All calculations were performed with the Gaussian09 program package.[85]

■ ASSOCIATED CONTENT

Supporting Information

The Supporting Information is available free of charge on the ACS Publications website at DOI: 10.1021/acs.chemmater.8b04278.

Synthetic procedures of all chelates, photoluminescence spectra of **m2h-3** and **m6h-3**, and electrochemical, thermal analysis, and photodegradation data of the studied Ir(III) metal complexes (PDF)

Molecular structure and selected metric parameters of **m2h-1** (CCDC entry 187240) (CIF)

Molecular structure and selected metric parameters of **m6h-1** (CCDC entry 187239) (CIF)

■ AUTHOR INFORMATION

Corresponding Author

*E-mail: yunchi@cityu.edu.hk.

ORCID

Chih-Hao Chang: 0000-0002-5586-9526

Daniel Escudero: 0000-0002-1777-8578

Alex K.-Y. Jen: 0000-0002-9219-7749

Yun Chi: 0000-0002-8441-3974

DOI: 10.1021/acs.chemmater.8b04278
Chem. Mater. XXXX, XXX, XXX−XXX

Notes

The authors declare no competing financial interest.

■ ACKNOWLEDGMENTS

This work was supported by funding from the Ministry of Science and Technology (MOST), a featured areas research program within the framework of the Higher Education Sprout Project administrated by Ministry of Education (MOE) of Taiwan, and the City University of Hong Kong.

■ REFERENCES

(1) Chi, Y.; Chou, P.-T. Transition Metal Phosphors with Cyclometalating Ligands; Fundamental and Applications. *Chem. Soc. Rev.* **2010**, *39*, 638−655.

(2) Xiang, H.; Cheng, J.; Ma, X.; Zhou, X.; Chruma, J. J. Near-Infrared Phosphorescence: Materials and Applications. *Chem. Soc. Rev.* **2013**, *42*, 6128−6185.

(3) Visbal, R.; Gimeno, M. C. N-Heterocyclic Carbene Metal Complexes: Photoluminescence and Applications. *Chem. Soc. Rev.* **2014**, *43*, 3551−3574.

(4) Li, K.; Ming Tong, G. S.; Wan, Q.; Cheng, G.; Tong, W.-Y.; Ang, W.-H.; Kwong, W.-L.; Che, C.-M. Highly Phosphorescent Platinum(II) Emitters: Photophysics, Materials and Biological Applications. *Chem. Sci.* **2016**, *7*, 1653−1673.

(5) Lu, C.-W.; Wang, Y.; Chi, Y. Metal Complexes with Azolate-Functionalized Multidentate Ligands: Tactical Designs and Optoelectronic Applications. *Chem. - Eur. J.* **2016**, *22*, 17892−17908.

(6) Baryshnikov, G.; Minaev, B.; Ågren, H. Theory and Calculation of the Phosphorescence Phenomenon. *Chem. Rev.* **2017**, *117*, 6500−6537.

(7) Wu, X.; Zhu, M.; Bruce, D. W.; Zhu, W.; Wang, Y. An Overview of Phosphorescent Metallomesogens Based on Platinum and Iridium. *J. Mater. Chem. C* **2018**, *6*, 9848−9860.

(8) Zhang, Y.; Wang, Y.; Song, J.; Qu, J.; Li, B.; Zhu, W.; Wong, W.-Y. Near-Infrared Emitting Materials Via Harvesting Triplet Excitons: Molecular Design, Properties, and Application in Organic Light Emitting Diodes. *Adv. Opt. Mater.* **2018**, *6*, 1800466.

(9) Hirata, S.; Sakai, Y.; Masui, K.; Tanaka, H.; Lee, S. Y.; Nomura, H.; Nakamura, N.; Yasumatsu, M.; Nakanotani, H.; Zhang, Q.; Shizu, K.; Miyazaki, H.; Adachi, C. Highly Efficient Blue Electroluminescence Based on Thermally Activated Delayed Fluorescence. *Nat. Mater.* **2015**, *14*, 330−336.

(10) Im, Y.; Byun, S. Y.; Kim, J. H.; Lee, D. R.; Oh, C. S.; Yook, K. S.; Lee, J. Y. Recent Progress in High-Efficiency Blue-Light-Emitting Materials for Organic Light-Emitting Diodes. *Adv. Funct. Mater.* **2017**, *27*, 1603007.

(11) Chen, Z.; Wang, L.; Su, S.; Zheng, X.; Zhu, N.; Ho, C.-L.; Chen, S.; Wong, W.-Y. Cyclometalated Iridium(III) Carbene Phosphors for Highly Efficient Blue Organic Light-Emitting Diodes. *ACS Appl. Mater. Interfaces* **2017**, *9*, 40497−40502.

(12) Wong, M. Y.; Zysman-Colman, E. Purely Organic Thermally Activated Delayed Fluorescence Materials for Organic Light-Emitting Diodes. *Adv. Mater.* **2017**, *29*, 1605444.

(13) Chan, C.-Y.; Cui, L.-S.; Kim, J. U.; Nakanotani, H.; Adachi, C. Rational Molecular Design for Deep-Blue Thermally Activated Delayed Fluorescence Emitters. *Adv. Funct. Mater.* **2018**, *28*, 1706023.

(14) Liu, Y.; Li, C.; Ren, Z.; Yan, S.; Bryce, M. R. All-Organic Thermally Activated Delayed Fluorescence Materials for Organic Light-Emitting Diodes. *Nat. Rev. Mater.* **2018**, *3*, 18020.

(15) Fu, H.; Cheng, Y.-M.; Chou, P.-T.; Chi, Y. Feeling Blue? Blue Phosphors for OLEDs. *Mater. Today* **2011**, *14*, 472−479.

(16) Song, W.; Lee, J. Y. Degradation Mechanism and Lifetime Improvement Strategy for Blue Phosphorescent Organic Light-Emitting Diodes. *Adv. Opt. Mater.* **2017**, *5*, 1600901.

(17) Cho, Y.-J.; Kim, S.-Y.; Kim, J.-H.; Crandell, D.; Baik, M.-H.; Lee, J.; Kim, C. H.; Son, H.-J.; Han, W.-S.; Kang, S. O. Important Role of Ancillary Ligand in the Emission Behaviours of Blue-Emitting Heteroleptic Ir(III) Complexes. *J. Mater. Chem. C* **2017**, *5*, 4480−4487.

(18) Li, X.; Zhang, J.; Zhao, Z.; Wang, L.; Yang, H.; Chang, Q.; Jiang, N.; Liu, Z.; Bian, Z.; Liu, W.; Lu, Z.; Huang, C. Deep Blue Phosphorescent Organic Light-Emitting Diodes with Ciey Value of 0.11 and External Quantum Efficiency up to 22.5%. *Adv. Mater.* **2018**, *30*, 1705005.

(19) Sajoto, T.; Djurovich, P. I.; Tamayo, A. B.; Oxgaard, J.; Goddard, W. A.; Thompson, M. E. Temperature Dependence of Blue Phosphorescent Cyclometalated Ir(III) Complexes. *J. Am. Chem. Soc.* **2009**, *131*, 9813−9822.

(20) Lee, J.; Chen, H.-F.; Batagoda, T.; Coburn, C.; Djurovich, P. I.; Thompson, M. E.; Forrest, S. R. Deep Blue Phosphorescent Organic Light-Emitting Diodes with Very High Brightness and Efficiency. *Nat. Mater.* **2016**, *15*, 92−98.

(21) Zhu, Z.-L.; Ni, S.-F.; Chen, W.; Chen, M.; Zhu, J.; Yuan, Y.; Tong, Q.-X.; Wong, F.-L.; Lee, C.-s. Tuning Electrical Properties of Phenanthroimidazole Derivatives to Construct Multifunctional Deep-Blue Electroluminescent Materials. *J. Mater. Chem. C* **2018**, *6*, 3584−3592.

(22) Kuei, C.-Y.; Liu, S.-H.; Chou, P.-T.; Lee, G.-H.; Chi, Y. Room Temperature Blue Phosphorescence; a Combined Experimental and Theoretical Study on the Bis-Tridentate Ir(III) Metal Complexes. *Dalton Trans.* **2016**, *45*, 15364−15373.

(23) Chi, Y.; Chang, T.-K.; Ganesan, P.; Rajakannu, P. Emissive Bis-Tridentate Ir(III) Metal Complexes: Tactics, Photophysics and Applications. *Coord. Chem. Rev.* **2017**, *346*, 91−100.

(24) Kuei, C.-Y.; Tsai, W.-L.; Tong, B.; Jiao, M.; Lee, W.-K.; Chi, Y.; Wu, C.-C.; Liu, S.-H.; Lee, G.-H.; Chou, P.-T. Bis-Tridentate Ir(III) Complexes with Nearly Unitary Rgb Phosphorescence and Organic Light-Emitting Diodes with External Quantum Efficiency Exceeding 31%. *Adv. Mater.* **2016**, *28*, 2795−2800.

(25) Kuo, H.-H.; Chen, Y.-T.; Devereux, L. R.; Wu, C.-C.; Fox, M. A.; Kuei, C.-Y.; Chi, Y.; Lee, G.-H. Bis-Tridentate Ir(III) Metal Phosphors for Efficient Deep-Blue Organic Light-Emitting Diodes. *Adv. Mater.* **2017**, *29*, 1702464.

(26) Kuo, H.-H.; Zhu, Z.-L.; Lee, C.-S.; Chen, Y.-K.; Liu, S.-H.; Chou, P.-T.; Jen, A. K.-Y.; Chi, Y. Bis-Tridentate Iridium(III) Phosphors with Very High Photostability and Fabrication of Blue-Emitting OLEDs. *Adv. Sci.* **2018**, *5*, 1800846.

(27) Su, S.-J.; Cai, C.; Kido, J. Rgb Phosphorescent Organic Light-Emitting Diodes by Using Host Materials with Heterocyclic Cores: Effect of Nitrogen Atom Orientations. *Chem. Mater.* **2011**, *23*, 274−284.

(28) Park, I. S.; Lee, J.; Yasuda, T. High-Performance Blue Organic Light-Emitting Diodes with 20% External Electroluminescence Quantum Efficiency Based on Pyrimidine-Containing Thermally Activated Delayed Fluorescence Emitters. *J. Mater. Chem. C* **2016**, *4*, 7911−7916.

(29) Wu, K.; Zhang, T.; Zhan, L.; Zhong, C.; Gong, S.; Jiang, N.; Lu, Z.-H.; Yang, C. Optimizing Optoelectronic Properties of Pyrimidine-Based Tadf Emitters by Changing the Substituent for Organic Light-Emitting Diodes with External Quantum Efficiency Close to 25% and Slow Efficiency Roll-Off. *Chem. - Eur. J.* **2016**, *22*, 10860−10866.

(30) Pan, K.-C.; Li, S.-W.; Ho, Y.-Y.; Shiu, Y.-J.; Tsai, W.-L.; Jiao, M.; Lee, W.-K.; Wu, C.-C.; Chung, C.-L.; Chatterjee, T.; Li, Y.-S.; Wong, K.-T.; Hu, H.-C.; Chen, C.-C.; Lee, M.-T. Efficient and Tunable Thermally Activated Delayed Fluorescence Emitters Having Orientation-Adjustable CN-Substituted Pyridine and Pyrimidine Acceptor Units. *Adv. Funct. Mater.* **2016**, *26*, 7560−7571.

(31) Ganesan, P.; Ranganathan, R.; Chi, Y.; Liu, X.-K.; Lee, C.-S.; Liu, S.-H.; Lee, G.-H.; Lin, T.-C.; Chen, Y.-T.; Chou, P.-T. Functional Pyrimidine-Based Thermally Activated Delay Fluorescence Emitters: Photophysics, Mechanochromism and Fabrication of Organic Light-Emitting Diodes. *Chem. - Eur. J.* **2017**, *23*, 2858−2866.

(32) Nakao, K.; Sasabe, H.; Komatsu, R.; Hayasaka, Y.; Ohsawa, T.; Kido, J. Significant Enhancement of Blue OLED Performances through Molecular Engineering of Pyrimidine-Based Emitter. *Adv. Opt. Mater.* **2017**, *5*, 1600843.

DOI: 10.1021/acs.chemmater.8b04278
Chem. Mater. XXXX, XXX, XXX−XXX

(33) Park, I. S.; Komiyama, H.; Yasuda, T. Pyrimidine-Based Twisted Donor-Acceptor Delayed Fluorescence Molecules: A New Universal Platform for Highly Efficient Blue Electroluminescence. *Chem. Sci.* **2017**, *8*, 953−960.
(34) Park, H.-J.; Han, S. H.; Lee, J. Y.; Han, H.; Kim, E.-G. Managing Orientation of Nitrogens in Bipyrimidine-Based Thermally Activated Delayed Fluorescent Emitters to Suppress Nonradiative Mechanisms. *Chem. Mater.* **2018**, *30*, 3215−3222.
(35) Hudson, Z. M.; Wang, Z.; Helander, M. G.; Lu, Z.-H.; Wang, S. N-Heterocyclic Carbazole-Based Hosts for Simplified Single-Layer Phosphorescent OLEDs with High Efficiencies. *Adv. Mater.* **2012**, *24*, 2922−2928.
(36) Lee, Y.-T.; Chang, Y.-T.; Lee, M.-T.; Chiang, P.-H.; Chen, C.-T.; Chen, C.-T. Solution-Processed Bipolar Small Molecular Host Materials for Single-Layer Blue Phosphorescent Organic Light-Emitting Diodes. *J. Mater. Chem. C* **2014**, *2*, 382−391.
(37) Kim, G. H.; Lampande, R.; Park, M. J.; Bae, H. W.; Kong, J. H.; Kwon, J. H.; Park, J. H.; Park, Y. W.; Song, C. E. Highly Efficient Bipolar Host Materials with Indenocarbazole and Pyrimidine Moieties for Phosphorescent Green Light-Emitting Diodes. *J. Phys. Chem. C* **2014**, *118*, 28757−28763.
(38) Sasabe, H.; Sato, R.; Suzuki, K.; Watanabe, Y.; Adachi, C.; Kaji, H.; Kido, J. Ultrahigh Power Efficiency Thermally Activated Delayed Fluorescent OLEDs by the Strategic Use of Electron-Transport Materials. *Adv. Opt. Mater.* **2018**, *6*, 1800376.
(39) Cui, L.-S.; Liu, Y.; Liu, X.-Y.; Jiang, Z.-Q.; Liao, L.-S. Design and Synthesis of Pyrimidine-Based Iridium(III) Complexes with Horizontal Orientation for Orange and White Phosphorescent OLEDs. *ACS Appl. Mater. Interfaces* **2015**, *7*, 11007−11014.
(40) Sarma, M.; Tsai, W.-L.; Lee, W.-K.; Chi, Y.; Wu, C.-C.; Liu, S.-H.; Chou, P.-T.; Wong, K.-T. Anomalously Long-Lasting Blue Pholed Featuring Phenyl-Pyrimidine Cyclometalated Iridium Emitter. *Chem.* **2017**, *3*, 461−476.
(41) Zhang, S.; Xia, J.-C.; Wu, Z.-G.; Lu, G.-Z.; Zhao, Y.; Zheng, Y.-X. Two Green-Phosphorescent Iridium Complexes with 2-Phenylpyrimidine Derivatives and Tetraphenylimidodiphosphinate for Efficient Organic Light-Emitting Diodes. *Eur. J. Inorg. Chem.* **2016**, *2016*, 2556−2561.
(42) Han, H.-B.; Wu, Z.-G.; Zheng, Y.-X. Efficient Electroluminescence of Bluish Green Iridium Complexes with 2-(3,5-Bis(Trifluoromethyl)Phenyl)Pyrimidine and 2-(3,5-Bis-(Trifluoromethyl)Phenyl)-5-Fluoropyrimidine as the Main Ligands. *Inorg. Chem. Front.* **2018**, *5*, 1545−1552.
(43) Jiang, B.; Zhao, C.; Ning, X.; Zhong, C.; Ma, D.; Yang, C. Using Simple Fused-Ring Thieno[2,3-D]Pyrimidine to Construct Orange/Red Ir(III) Complexes: High-Performance Red Organic Light-Emitting Diodes with Eqes up to Nearly 28%. *Adv. Opt. Mater.* **2018**, *6*, 1800108.
(44) Deng, Y.-L.; Cui, L.-S.; Liu, Y.; Wang, Z.-K.; Jiang, Z.-Q.; Liao, L.-S. Solution-Processable Iridium Phosphors for Efficient Red and White Organic Light-Emitting Diodes with Low Roll-Off. *J. Mater. Chem. C* **2016**, *4*, 1250−1256.
(45) Tong, B.-H.; Mei, Q.-B.; Tian, R.-Q.; Yang, M.; Hua, Q.-F.; Shi, Y.-J.; Ye, S.-H. High-Brightness Solution-Processed Phosphorescent OLEDs with Pyrimidine-Based Iridium(III) Complexes. *RSC Adv.* **2016**, *6*, 34970−34976.
(46) Mei, Q.; Chen, C.; Tian, R.; Yang, M.; Tong, B.; Hua, Q.; Shi, Y.; Fan, Q.; Ye, S. Highly Efficient Orange Phosphorescent Organic Light-Emitting Diodes Based on an Iridium(III) Complex with Diethyldithiocarbamate (S^S) as the Ancillary Ligand. *RSC Adv.* **2016**, *6*, 64003−64008.
(47) Vargas, V. C.; Rubio, R. J.; Hollis, T. K.; Salcido, M. E. Efficient Route to 1,3-Di-N-Imidazolylbenzene. A Comparison of Monodentate Vs. Bidentate Carbenes in Pd-Catalyzed Cross Coupling. *Org. Lett.* **2003**, *5*, 4847−4849.
(48) Lanoe, P.-H.; Tong, C. M.; Harrington, R. W.; Probert, M. R.; Clegg, W.; Williams, J. A. G.; Kozhevnikov, V. N. Ditopic Bis-Terdentate Cyclometallating Ligands and Their Highly Luminescent Dinuclear Iridium(III) Complexes. *Chem. Commun.* **2014**, *50*, 6831−6834.
(49) Yang, X.; Xu, X.; Dang, J.-s.; Zhou, G.; Ho, C.-L.; Wong, W.-Y. From Mononuclear to Dinuclear Iridium(III) Complex: Effective Tuning of the Optoelectronic Characteristics for Organic Light-Emitting Diodes. *Inorg. Chem.* **2016**, *55*, 1720−1727.
(50) Yang, X.; Feng, Z.; Zhao, J.; Dang, J.-S.; Liu, B.; Zhang, K.; Zhou, G. Pyrimidine-Based Mononuclear and Dinuclear Iridium(III) Complexes for High Performance Organic Light-Emitting Diodes. *ACS Appl. Mater. Interfaces* **2016**, *8*, 33874−33887.
(51) Daniels, R. E.; Culham, S.; Hunter, M.; Durrant, M. C.; Probert, M. R.; Clegg, W.; Williams, J. A. G.; Kozhevnikov, V. N. When Two Are Better Than One: Bright Phosphorescence from Non-Stereogenic Dinuclear Iridium(III) Complexes. *Dalton Trans.* **2016**, *45*, 6949−6962.
(52) Liu, Z.; Cao, F.; Tsuboi, T.; Yue, Y.; Deng, C.; Ni, X.; Sun, W.; Zhang, Q. High Fluorescence Rate as a Key for Stable Blue Organic Light-Emitting Diodes. *J. Mater. Chem. C* **2018**, *6*, 7728−7733.
(53) Sajoto, T.; Djurovich, P. I.; Tamayo, A.; Yousufuddin, M.; Bau, R.; Thompson, M. E.; Holmes, R. J.; Forrest, S. R. Blue and near-UV Phosphorescence from Iridium Complexes with Cyclometalated Pyrazolyl or N-Heterocyclic Carbene Ligands. *Inorg. Chem.* **2005**, *44*, 7992−8003.
(54) Yang, C.-H.; Cheng, Y.-M.; Chi, Y.; Hsu, C.-J.; Fang, F.-C.; Wong, K.-T.; Chou, P.-T.; Chang, C.-H.; Tsai, M.-H.; Wu, C.-C. Blue-Emitting Heteroleptic Iridium(III) Complexes Suited for High Efficiency Phosphorescent OLEDs. *Angew. Chem., Int. Ed.* **2007**, *46*, 2418−2421.
(55) Cho, Y.-J.; Kim, S.-Y.; Kim, J.-H.; Lee, J.; Cho, D. W.; Yi, S.; Son, H.-J.; Han, W.-S.; Kang, S. O. Probing Photophysical Properties of Isomeric N-Heterocyclic Carbene Ir(III) Complexes and Their Applications to Deep Blue Phosphorescent Organic Light-Emitting Diodes. *J. Mater. Chem. C* **2017**, *5*, 1651−1659.
(56) Arroliga-Rocha, S.; Escudero, D. Facial and Meridional Isomers of Tris(Bidentate) Ir(III) Complexes: Unravelling Their Different Excited State Reactivity. *Inorg. Chem.* **2018**, *57*, 12106−12112.
(57) Chang, C.-H.; Chen, C.-C.; Wu, C.-C.; Yang, C.-H.; Chi, Y. Efficient Iridium(III) Based, True-Blue Emitting Phosphorescent OLEDs Employing Both Double Emission and Double Buffer Layers. *Org. Electron.* **2009**, *10*, 1364−1371.
(58) Liao, J.-L.; Chi, Y.; Sie, Z.-T.; Ku, C.-H.; Chang, C.-H.; Fox, M. A.; Low, P. J.; Tseng, M.-R.; Lee, G.-H. Ir(III)-Based Phosphors with Bipyrazolate Ancillaries; Rational Design, Photophysics, and Applications in Organic Light-Emitting Diodes. *Inorg. Chem.* **2015**, *54*, 10811−10821.
(59) Baldo, M. A.; Adachi, C.; Forrest, S. R. Transient Analysis of Organic Electrophosphorescence. II. Transient Analysis of Triplet-Triplet Annihilation. *Phys. Rev. B: Condens. Matter Mater. Phys.* **2000**, *62*, 10967−10977.
(60) Murawski, C.; Leo, K.; Gather, M. C. Efficiency Roll-Off in Organic Light-Emitting Diodes. *Adv. Mater.* **2013**, *25*, 6801−6827.
(61) Su, S.-J.; Gonmori, E.; Sasabe, H.; Kido, J. Highly Efficient Organic Blue-and White-Light-Emitting Devices Having a Carrier- and Exciton-Confining Structure for Reduced Efficiency Roll-Off. *Adv. Mater.* **2008**, *20*, 4189−4194.
(62) Chang, C.-H.; Wu, Z.-J.; Chiu, C.-H.; Liang, Y.-H.; Tsai, Y.-S.; Liao, J.-L.; Chi, Y.; Hsieh, H.-Y.; Kuo, T.-Y.; Lee, G.-H.; Pan, H.-A.; Chou, P.-T.; Lin, J.-S.; Tseng, M.-R. A New Class of Sky-Blue-Emitting Ir(III) Phosphors Assembled Using Fluorine-Free Pyridyl Pyrimidine Cyclometalates: Application toward High-Performance Sky-Blue- and White-Emitting OLEDs. *ACS Appl. Mater. Interfaces* **2013**, *5*, 7341−7351.
(63) Su, S.-J.; Sasabe, H.; Takeda, T.; Kido, J. Pyridine-Containing Bipolar Host Materials for Highly Efficient Blue Phosphorescent OLEDs. *Chem. Mater.* **2008**, *20*, 1691−1693.
(64) Cai, C.; Su, S.-J.; Chiba, T.; Sasabe, H.; Pu, Y.-J.; Nakayama, K.; Kido, J. High-Efficiency Red, Green and Blue Phosphorescent Homojunction Organic Light-Emitting Diodes Based on Bipolar Host Materials. *Org. Electron.* **2011**, *12*, 843−850.

DOI: 10.1021/acs.chemmater.8b04278
Chem. Mater. XXXX, XXX, XXX−XXX

(65) Hung, W.-Y.; Fang, G.-C.; Chang, Y.-C.; Kuo, T.-Y.; Chou, P.-T.; Lin, S.-W.; Wong, K.-T. Highly Efficient Bilayer Interface Exciplex for Yellow Organic Light-Emitting Diode. *ACS Appl. Mater. Interfaces* **2013**, *5*, 6826−6831.
(66) Song, W.; Lee, H. L.; Lee, J. Y. High Triplet Energy Exciplex Hosts for Deep Blue Phosphorescent Organic Light-Emitting Diodes. *J. Mater. Chem. C* **2017**, *5*, 5923−5929.
(67) Han, C.; Zhao, Y.; Xu, H.; Chen, J.; Deng, Z.; Ma, D.; Li, Q.; Yan, P. A Simple Phosphine-Oxide Host with a Multi-Insulating Structure: High Triplet Energy Level for Efficient Blue Electrophosphorescence. *Chem. - Eur. J.* **2011**, *17*, 5800−5803.
(68) Xu, H.; Wang, L.-H.; Zhu, X.-H.; Yin, K.; Zhong, G.-Y.; Hou, X.-Y.; Huang, W. Application of Chelate Phosphine Oxide Ligand in Eu^{III} Complex with Mezzo Triplet Energy Level, Highly Efficient Photoluminescent, and Electroluminescent Performances. *J. Phys. Chem. B* **2006**, *110*, 3023−3029.
(69) Lin, C.-H.; Chang, Y.-Y.; Hung, J.-Y.; Lin, C.-Y.; Chi, Y.; Chung, M.-W.; Lin, C.-L.; Chou, P.-T.; Lee, G.-H.; Chang, C.-H.; Lin, W.-C. Ir^{III} Complexes Bearing Dicyclometalated Phosphite Tripod; Strategy to Achieve Blue Phosphorescence Free from Fluorine Substituent and Fabrication of OLEDs. *Angew. Chem., Int. Ed.* **2011**, *50*, 3182−3186.
(70) Liao, K.-Y.; Hsu, C.-W.; Chi, Y.; Hsu, M.-K.; Wu, S.-W.; Chang, C.-H.; Liu, S.-H.; Lee, G.-H.; Chou, P.-T.; Hu, Y.; Robertson, N. Pt(II) Metal Complexes Tailored with a Newly Designed Spiro-Arranged Tetradentate Ligand; Harnessing of Charge-Transfer Phosphorescence and Fabrication of Sky Blue and White OLEDs. *Inorg. Chem.* **2015**, *54*, 4029−4038.
(71) Su, S.-J.; Chiba, T.; Takeda, T.; Kido, J. Pyridine-Containing Triphenylbenzene Derivatives with High Electron Mobility for Highly Efficient Phosphorescent OLEDs. *Adv. Mater.* **2008**, *20*, 2125−2130.
(72) Su, S.-J.; Takahashi, Y.; Chiba, T.; Takeda, T.; Kido, J. Structure-Property Relationship of Pyridine-Containing Triphenyl Benzene Electron-Transport Materials for Highly Efficient Blue Phosphorescent OLEDs. *Adv. Funct. Mater.* **2009**, *19*, 1260−1267.
(73) Lee, S.; Lee, J.-H.; Lee, J.-H.; Kim, J.-J. The Mechanism of Charge Generation in Charge-Generation Units Composed of P-Doped Hole-Transporting Layer/HATCN/N-Doped Electron-Transporting Layers. *Adv. Funct. Mater.* **2012**, *22*, 855−860.
(74) Park, Y.-S.; Lee, S.; Kim, K.-H.; Kim, S.-Y.; Lee, J.-H.; Kim, J.-J. Exciplex-Forming Co-Host for Organic Light-Emitting Diodes with Ultimate Efficiency. *Adv. Funct. Mater.* **2013**, *23*, 4914−4920.
(75) Lin, J.; Chau, N.-Y.; Liao, J.-L.; Wong, W.-Y.; Lu, C.-Y.; Sie, Z.-T.; Chang, C.-H.; Fox, M. A.; Low, P. J.; Lee, G.-H.; Chi, Y. Bis-Tridentate Iridium(III) Phosphors Bearing Functional 2-Phenyl-6-(Imidazol-2-Ylidene)Pyridine and 2-(Pyrazol-3-Yl)-6-Phenylpyridine Chelates for Efficient OLEDs. *Organometallics* **2016**, *35*, 1813−1824.
(76) Chen, D.-G.; Lin, T.-C.; Chen, C.-L.; Chen, Y.-T.; Chen, Y.-A.; Lee, G.-H.; Chou, P.-T.; Liao, C.-W.; Chiu, P.-C.; Chang, C.-H.; Lien, Y.-J.; Chi, Y. Optically Triggered Planarization of Boryl-Substituted Phenoxazine: Another Horizon of Tadf Molecules and High-Performance OLEDs. *ACS Appl. Mater. Interfaces* **2018**, *10*, 12886−12896.
(77) Sasabe, H.; Takamatsu, J.; Motoyama, T.; Watanabe, S.; Wagenblast, G.; Langer, N.; Molt, O.; Fuchs, E.; Lennartz, C.; Kido, J. High-Efficiency Blue and White Organic Light-Emitting Devices Incorporating a Blue Iridium Carbene Complex. *Adv. Mater.* **2010**, *22*, 5003−5007.
(78) Tseng, C.-H.; Fox, M. A.; Liao, J.-L.; Ku, C.-H.; Sie, Z.-T.; Chang, C.-H.; Wang, J.-Y.; Chen, Z.-N.; Lee, G.-H.; Chi, Y. Luminescent Pt(II) Complexes Featuring Imidazolylidene-Pyridylidene and Dianionic Bipyrazolate: From Fundamentals to OLED Fabrications. *J. Mater. Chem. C* **2017**, *5*, 1420−1435.
(79) Hertel, D.; Meerholz, K. Triplet-Polaron Quenching in Conjugated Polymers. *J. Phys. Chem. B* **2007**, *111*, 12075−12080.
(80) Erickson, N. C.; Holmes, R. J. Engineering Efficiency Roll-Off in Organic Light-Emitting Devices. *Adv. Funct. Mater.* **2014**, *24*, 6074−6080.
(81) Becke, A. D. Density-Functional Thermochemistry. Iii. The Role of Exact Exchange. *J. Chem. Phys.* **1993**, *98*, 5648−5652.
(82) Lee, C.; Yang, W.; Parr, R. G. Development of the Colle-Salvetti Correlation-Energy Formula into a Functional of the Electron Density. *Phys. Rev. B: Condens. Matter Mater. Phys.* **1988**, *37*, 785−789.
(83) Andrae, D.; Häußermann, U.; Dolg, M.; Stoll, H.; Preuß, H. Energy-Adjusted ab Initio Pseudopotentials for the Second and Third Row Transition Elements. *Theor. Chim. Acta* **1990**, *77*, 123−141.
(84) Tomasi, J.; Mennucci, B.; Cammi, R. Quantum Mechanical Continuum Solvation Models. *Chem. Rev.* **2005**, *105*, 2999−3094.
(85) Frisch, M. J.; Trucks, G. W.; Schlegel, H. B.; Scuseria, G. E.; Robb, M. A.; Cheeseman, J. R.; Scalmani, G.; Barone, V.; Mennucci, B.; Petersson, G. A.; Nakatsuji, H.; Caricato, M.; Li, X.; Hratchian, H. P.; Izmaylov, A. F.; Bloino, J.; Zheng, G.; Sonnenberg, J. L.; Hada, M.; Ehara, M.; Toyota, K.; Fukuda, R.; Hasegawa, J.; Ishida, M.; Nakajima, T.; Honda, Y.; Kitao, O.; Nakai, H.; Vreven, T.; Montgomery, J. A., Jr.; Peralta, J. E.; Ogliaro, F.; Bearpark, M.; Heyd, J. J.; Brothers, E.; Kudin, K. N.; Staroverov, V. N.; Kobayashi, R.; Normand, J.; Raghavachari, K.; Rendell, A.; Burant, J. C.; Iyengar, S. S.; Tomasi, J.; Cossi, M.; Rega, N.; Millam, J. M.; Klene, M.; Knox, J. E.; Cross, J. B.; Bakken, V.; Adamo, C.; Jaramillo, J.; Gomperts, R.; Stratmann, R. E.; Yazyev, O.; Austin, A. J.; Cammi, R.; Pomelli, C.; Ochterski, J. W.; Martin, R. L.; Morokuma, K.; Zakrzewski, V. G.; Voth, G. A.; Salvador, P.; Dannenberg, J. J.; Dapprich, S.; Daniels, A. D.; Farkas, Ö.; Foresman, J. B.; Ortiz, J. V.; Cioslowski, J.; Fox, D. J. *Gaussian 09*, revision D.01; Gaussian, Inc.: Wallingford, CT, 2013.

DOI: 10.1021/acs.chemmater.8b04278
Chem. Mater. XXXX, XXX, XXX−XXX